Optimization-based Wideband Basis Functions for Efficient Interconnect Extraction

Xin Hu[*], Tarek Moselhy[†], Jacob White[†],and Luca Daniel[†]
[*]Ropes and Gray LLP
Boston, MA
Email: xinhu@alum.mit.edu
[†]Research Laboratory in Electronics
Massachusetts Institute of Technology
77 Massachusetts Ave,
Cambridge, MA, 02139

Abstract— This paper introduces a technique for the numerical generation of basis functions that are capable of parameterizing the frequency-variant nature of cross-sectional conductor current distributions. Hence skin and proximity effects can be captured utilizing much fewer basis functions in comparison to the prevalently-used piecewise-constant basis functions. One important characteristic of these basis functions is that they only need to be pre-computed once for a frequency range of interest per unique conductor cross-sectional geometry, and they can be stored off-line with a minimal associated cost. In addition, the robustness of these frequency-independent basis functions are enforced using an optimization routine. It has been demonstrated that the cost of solving a complex interconnect system can be reduced by a factor of 170 when compared to the use of piecewise-constant basis functions over a wide range of operating frequencies.

I. INTRODUCTION

To date, there exists numerous accelerated integral-equation based electromagnetic solvers [1], [2], [3], [4], [5], [6] that are capable of rapid and accurate resolution of large conductor system impedance, some of which can even account for the effects invoked by the presence of a semi-conductive substrate. However, the efficiency of these solvers is being continuously challenged by the ever increasing operating frequencies which generate skin and proximity effects that need to be carefully modeled in order to provide accurate impedance solutions.

Skin and proximity effects are troublesome for today's fast solvers due to the fact that most of the mixed potential integral equation (MPIE) solvers rely on piecewise-constant [7], [2], [6] or piecewise-linear basis functions to capture conductor current distributions. As frequency increases, the use of these basis functions has proven to be computationally expensive because a very fine discretization scheme must be applied in order to faithfully capture the exponential variation in cross-sectional conductor current, thus generating densely-populated clusters of filaments with highly uneven aspect ratios. One might think this is not problematic if the discretized system were to be solved by a fast technique since, theoretically speaking, the computational cost only scales in a linear fashion with the total number of basis functions. However, in practice, direct computation must be used to account for the numerous near-distanced interactions generated by clusters of long and skinny filaments which takes a quadratic order of complexity to resolve.

The explosive cost associated with high-frequency impedance simulations has spurred the development of methods that seek to either represent interior conductor current using surface field quantities [8], [9], [10], [11], [5] or generate specialized basis functions that have the built-in capability of capturing interior current variations [12], [13]. However, major drawbacks have been observed in the first approach where surface-based formulations such as [11], [5] result in excessively complex systems that are numerical unstable at low-frequencies. Therefore, for the sake of accuracy and robustness of implementation, the latter of the two approaches is preferred. Specifically, according to [12], a set of specialized basis functions called "conduction modes" is analytically derived from the interior Helmholtz equations governing the flow of longitudinal current through a conductor. One distinct disadvantage of these specialized basis functions is that they can only be generated for those cross-section shapes where analytical solutions of the diffusion equation are available. Practically speaking, only rectangular and cylindrical cross-sections can be handled. Another disadvantage of the conduction mode basis functions is that they are incapable of capturing proximity effects in neighboring wires of dissimilar cross-sectional shapes. To remedy these shortcomings, [13] describes another set of basis functions called "proximity templates" that is pre-computed numerically at each desired frequency for each unique conductor cross-section type. An apparent disadvantage of such an approach is the high computational cost associated with constructing these basis functions if there exists a large number of frequency points of interest. Another disadvantage is the lack of predictability in the method's accuracy due to the fact that its solutions are entirely dependent on the judicious placement of only a handful of trial samples.

In this paper, a set of basis functions is introduced that maximizes the efficiency with which large and complex interconnect structures are modeled. According to the procedure outlined in Sec. III, these basis functions only need to be pre-computed once per conductor cross-section geometry of interest. One of the major and novel contributions is that these basis are valid for a wide range of frequencies of operation. For the sake of reusability, these basis functions can be stored off-line with a minimal storage cost. In spite of having the advantage of being inherently frequency-independent within a given frequency range, these basis functions are also able to collectively parameterize the frequency-variant nature of conductor current distributions, hence providing reasonably accurate modeling solutions with far fewer degrees of freedom in comparison to the use of traditional basis functions. Furthermore, a second key contribution is that post-optimization techniques are applied to the resulting basis functions in order to guarantee their numerical robustness and avoid system illconditioning. In addition, these basis functions will not complicate the cost of volume integrations in a Galerkin scheme [7] if a mixed-potential integral-equation (MPIE) formulation were used. In Section IV, examples are presented to demonstrate the superior efficiency with which the specialized basis functions perform impedance extractions of complex interconnect systems when implemented in a MPIE fast solver that also accounts for substrate effects [2].

II. BACKGROUND

A. MPIE Formulation

As in [2], [7], [6], the following set of integral equations can be used to compute conductor volume current density $\overline{J}$ and conductor surface charge density ρ,

$$\frac{\overline{J}(r)}{\sigma} + j\omega\frac{\mu}{4\pi}\int_v \overline{\overline{G}}_A(r,r')\overline{J}(r')dr' = -\nabla\phi(r) \qquad (1)$$

$$\frac{1}{4\pi\varepsilon}\int_s G_\phi(r,r')\rho(r')dr' = \phi(r) \qquad (2)$$

$$\nabla\cdot\overline{J}(r) = 0 \qquad (3)$$

$$\hat{n}\cdot\overline{J}(r) = j\omega\rho(r), \qquad (4)$$

where v and s are the union of conductor volumes and surfaces respectively, ϕ is the scalar surface potential, μ is the magnetic permeability, ε is the dielectric constant, σ is the conductivity, and ω is the angular frequency of the conductor excitation. Vector and scalar layered Green's functions $\overline{\overline{G}}_A$ and G_ϕ account for conductor potentials under the influence of a semi-conductive substrate. Details regarding their derivation can be found in [2].

B. Discretization

For a given interconnect structure, after specifying a set of terminal voltages as inputs, (1)-(4) can be solved numerically for the current density $\overline{J}$ and charge density ρ. The standard approach for such computation is to approximate each type of unknowns by a weighted sum of a finite number of basis functions such that, for the calculation of current density vector:

$$\overline{J}(r) \approx \sum_j \overline{m}_j(r)I_j, \qquad (5)$$

where $\overline{m}_j \in C^3$ is a current density basis function, and I_j is its corresponding basis function weight. Similarly, for the charge density calculation, $\rho(r) \approx \sum_m v_m(r)q_m$, where $v_m \in C$ and q_m denotes a charge density basis function and its weight, respectively. A Galerkin technique [14] can then be used to generate a discrete system of equations for the weights according to the derivation in [12], [13]. The resulting linear system is expressed as follows:

$$\begin{bmatrix} R+j\omega L & 0 \\ 0 & \frac{P}{j\omega} \end{bmatrix}\begin{bmatrix} I \\ I_p \end{bmatrix} = \begin{bmatrix} V \\ V_\phi \end{bmatrix}, \qquad (6)$$

where I is a vector of current density basis function weights, and I_p is a displacement current vector that is related to charge density basis function weights in vector q through the relation $I_p = j\omega q$. Sub-matrices of the above system matrix are defined as:

$$R_{ij} = \frac{1}{\sigma}\int_v \overline{m}_i(r)\cdot\overline{m}_j(r)dr \qquad (7)$$

$$L_{ij} = \int_v\int_v \overline{\overline{G}}_A(r,r')\overline{m}_i(r)\cdot\overline{m}_j(r')dr'dr \qquad (8)$$

$$P_{m\ell} = \int_s\int_s G_\phi(r,r')v_m(r)v_\ell(r')dr'dr. \qquad (9)$$

To solve (6), the matrix equation is first mapped onto an equivalent circuit topology as described in [6], yielding the following matrix branch equation:

$$ZI_b = V_b, \qquad (10)$$

where impedance matrix Z, branch current vector I_b, and branch voltage vector V_b bear one-to-one correspondences to matrix quantities in (6). Equation (10) can then be combined with the remaining MPIE equations (3) and (4) through the imposition of mesh analysis [6] to produce a dense linear system for the basis function weights. More specifically, branch voltages in V_b can be related to loop voltages in V_m through the relation:

$$MV_b = V_m, \qquad (11)$$

where mesh matrix M imposes Kirchoff Voltage Law (KVL) at each row of M. The same M also maps branch currents in I_b to their corresponding loop currents in I_m through the relation

$$I_b = M^T I_m. \qquad (12)$$

Substituting (11) and (12) into (10) generates a meshed system that can be solved by an iterative method coupled with an accelerated matrix-vector product technique [1], [2], [3], [4], [5]. The solution of I_m subsequently allows one to determine branch currents in I_b that contains the actual basis function weights.

C. Current Density Basis Functions

To provide physical support for the collection of current density basis functions $\overline{m}_j$, the conductor volumes must be discretized accordingly. First, each conductor volume is discretized lengthwise into individually conducting segments with the assumption that a constant current flows in a length-wise direction through the segments. The number of segments produced per conductor is dictated by the magnitude of wavelength.

If basis function $\overline{m}_j$ were piecewise constant [7], [6], then the interior of each segment should also be discretized on its cross-section in a manner dictated by skin depth [13]. Bundles of many tightly-packed parallel filaments with highly uneven aspect ratios are generated per segment as a consequence of such discretization at high frequencies. The resulting filament-to-filament interactions within each segment, however, cannot be accelerated by today's fast techniques that are based on the approximation of distant interactions only. Therefore direct computations must be used to resolve these near-distanced interactions with a complexity that grows quadratically with the number of filaments per segment.

Hence it is extremely advantageous if higher-order basis can be developed that require much fewer functions to capture the cross-sectional current variation inherent in the segments. A general expression for a high-order current-density basis function $\overline{m}_j$ can be written as follows:

$$\overline{m}_j(r) = \begin{cases} \frac{W_j(r)\hat{l}_j}{\int_{a_j} W_j(r)dr} & \text{if } r \in V_j; \\ 0 & \text{otherwise,} \end{cases} \qquad (13)$$

where $\hat{l}_j$ is the length-wise direction of current flow in the jth segment, a_j is its cross-sectional area, and W_j returns the amount of current at a specific location on the segment's cross section. Each basis function $\overline{m}_j$ is normalized by a factor $\frac{1}{\int_{a_j} W_j(r)dr}$ in order to ensure that the corresponding basis function weight represents the actual branch current component flowing in filament j. The basis function representation in (13) is substituted into (7) to generate the following partial resistance:

$$R_{ij} = \frac{1}{\sigma\int_{a_i} W_i(r)dr\int_{a_j} W_j(r)dr}\int_{v_i} W_i(r)W_j(r)\hat{l}_i\cdot\hat{l}_jdr. \qquad (14)$$

Thus $R_{ij} \neq 0$ if and only if basis functions m_i and m_j are defined on the same conductor segment. Similarly, (13) is substituted into (8) to generate the following partial inductance:

$$L_{ij} = \frac{1}{\int_{a_i} W_i(r)dr\int_{a_j} W_j(r)dr}\int_{v_i}\int_{v_j} \overline{\overline{G}}_A(r,r')W_i(r)W_j(r)\hat{l}_i\cdot\hat{l}_jdr'dr. \qquad (15)$$
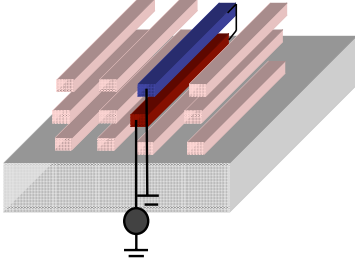
Fig. 1. Example of a possible source and test conductor pair for the construction of specialized basis functions that capture skin and proximity effects in a conductor's cross-section.

III. DEVELOPMENT OF THE WIDEBAND BASIS FUNCTIONS

This section describes the construction of a set of high-order basis that minimizes the number of functions per segment, parameterizes the frequency-dependent nature of current variation unique to different cross-section shapes, and guarantees frequency-independence for a wide range of frequencies.

A. Pre-computation of Basis Functions

A procedure for the automatic basis function generation is presented as follows:

1. For a given conductor of a specific cross-section shape, let's call this conductor a "source" conductor, consider placing another conductor, called "test" conductor, at a certain interaction distance r_i from the source conductor. Shorting the conductors at one end while exciting the structure with a unity current source at a desired frequency point would allow one to examine the current distribution over the cross section of the source conductor in response to the proximity effect generated by the test conductor at position r_i. Fig. 1 shows an example of such source and test conductor pair.

   The resulting solution of source current response v_i is obtained by using a very fine piecewise constant discretization method, hence producing η filaments per conductor segment. Extending this concept to p such test conductors situated at various locations surrounding the source conductor, one would thus obtain, for a specific excitation frequency, a collection V of such current solutions for the source conductor with $V = \{\bar{v}_i\}, i = 1 \ldots p$, and each vector $\bar{v}_i$ is of length η. If the spatial sampling of the test conductors is sufficiently fine, matrix V would contain a relevant set of "snapshots" from which proximity effects for a specific cross-section shape at a specific frequency can be captured. This step of the procedure is the same as the basis function generation procedure in [13].

2. Now select a set of frequency samples $S^n = \{s^1, s^2, \ldots, s^n\}$ at which step 1 is repeated. It becomes crucial that S^n spans the entire range of desired operating frequencies. In addition, the frequency samples should be fine enough so that the interpolation of the resulting sampled currents faithfully captures their overall variation with frequency. The combination of such spatial and frequency sampling subsequently generates a collection V_{pn} of source current solutions with $V_{pn} = \{\bar{v}_i\}, i = 1 \ldots p \times n$.

3. It becomes evident that the span of matrix V_{pn} captures a conductor's cross-sectional current distribution, accounting for both frequency-dependent skin effects and frequency plus spatial-dependent proximity effects. Therefore the subspace spanned by V_{pn} can be used to generate a set of specialized basis functions. More specifically, let's determine q ($q \ll p \times n$, $q \ll \eta$) such linearly-independent basis functions, the collection of which, $U = \{\bar{u}_1, \bar{u}_2, \ldots \bar{u}_q\}$, approximates V_{pn}. The accuracy of the approximation is measured by the minimal distance, in a least square sense, between the span of U and V_{pn}. To satisfy this minimization requirement, a singular-value-decomposition (SVD) method is used to generate these q orthogonal basis functions from the q dominant singular vectors of V_{pn}. Each one of these q basis functions can be viewed as a mode representing an orthogonally-decomposed current distribution shape over a conductor's cross section. Therefore a weighted sum of these current distribution modes is capable of accounting for the cross-sectional current distribution at any particular frequency point within the range from which the basis functions are generated.

In practice, at most 8 of these specialized basis functions ($q = 8$) are needed to accurately capture current distributions in most cross-section shapes over a wide span of frequencies. In contrast, a much larger number ($\eta \gg 8$) of piecewise-constant basis functions is needed to capture the cross-sectional current variation at one frequency point, and this number grows rapidly with the increase in frequency. In addition, the frequency-independent nature of the specialized basis functions implies that they only need to be pre-computed once for each unique cross-section geometry and can be stored off-line for repeated use. Since the number of these basis functions is small, storage cost is negligible.

B. Post-optimization of Basis Functions

In this section, we will demonstrate how optimization can be applied to the set of basis functions $U = \{\bar{u}_1 \ldots \bar{u}_q\}$ constructed from the previous section in order to avoid numerical difficulties encountered when these basis functions are used to approximate unknown current densities in a conductor system.

According to (5), the current density distribution in the ith conductor segment can be approximated by a weighted sum of the basis functions in U as:

$$\bar{J}_i \approx \sum_{j=1}^{q} \frac{\bar{u}_j \hat{\ell}_i}{ones(\eta)^T \bar{u}_j} I_j^i, \tag{16}$$

where the current variation unique to a cross-section shape can now be effectively captured by the span of U within a given frequency range. Coefficient I_j^i denotes the weight corresponding to the jth basis function ($\bar{u}_j$) as it contributes to the overall current distribution in segment i. In turn, each $\bar{u}_j$ is a vector of η piecewise-constant filament currents, the sum of which provides an accurate approximation of the cross-sectional current contained in the jth basis function mode. In order to ensure that such current is in general nonzero, we post-process the basis functions as follows:

Given a basis function matrix $U = \{\bar{u}_i, i=1..q\}$, where U is an orthonormal matrix with possible column sums being zero, we need to determine a set of coefficients $\{\alpha_{ij}, i=1..q, j=1..q\}$ such that

$$\bar{m}_j = \sum_{i=1}^{q} \alpha_{ij} \bar{u}_i, \tag{17}$$

where $\bar{m}_j$ forms a column of a new basis function matrix $M = \{\bar{m}_j, j=1..q\}$. M is subjected to the following constraints in terms of α:

- *Orthogonality:* ($\bar{m}_k \cdot \bar{m}_\ell = 0$ if $k > \ell$)

$$-\varepsilon < \left(\sum_{i=1}^{q} \alpha_{ik} \bar{u}_i \right)^T \left(\sum_{i=1}^{q} \alpha_{i\ell} \bar{u}_i \right) < \varepsilon \ \ if \ k > \ell, \tag{18}$$

  where ε is a small constant.
- *Nonzero column sums:* ($\sum \bar{m}_j > \beta$)

$$\left| \left(\sum_{i=1}^{q} \alpha_{ik} \bar{u}_i \right)^T ones(\eta) \right| > \beta, \tag{19}$$

  where β is a positive non-zero threshold constant and $ones(\eta)$ is a η-length vector of one's.

The problem is now formulated in such a manner that a standard optimization technique can be applied to solve the q^2 unknown α's, thus yielding a new ortho-normal basis function matrix M having the same span as the original matrix U, but guaranteeing nonzero column sums.

C. Incorporation of Basis Functions into MPIE

This section demonstrates how the collection of such modal basis functions, obtained using the procedure in Sec. III-A and optimized using the method in Sec. III-B, is incorporated into the MPIE formulation to produce a reduced system of equations for the potentials of a large interconnect network.

After replacing U in (16) by the optimized set of basis functions $M(= \{\overline{m}_j\}; j = 1 \dots q)$, one is able to use the new basis functions in a Galerkin technique to produce a linear system of equations for the unknown basis function weights. Let's examine the detail of this process. To obtain partial resistance R_{ij} in (14) in terms of basis function vectors $\overline{m}_i$ and $\overline{m}_j$, the following approximation can be made:

$$R_{ij} \approx \frac{1}{\sigma \sum_{k=1}^{\eta} m_{i_k} \sum_{k=1}^{\eta} m_{j_k}} \sum_{k=1}^{\eta} m_{i_k} m_{j_k} \frac{l_{i_k}}{a_{i_k}}, \quad (20)$$

where the η piecewise-constant current values in each basis function vector are considered to be discrete samplings of a continuous modal cross-sectional current distribution. Value m_{i_k} is the kth piecewise-constant current in the ith mode, l_{i_k} and a_{i_k} are the length and cross-sectional area, respectively, of the filament on which the kth piecewise-constant current of the ith mode is defined. If there are n conductor segments in the discretized system and q basis function modes for each segment, then R is a block-diagonal matrix of size $qn \times qn$ with each block being $q \times q$.

Similarly, for the calculation of partial inductance L_{ij} in (15):

$$L_{ij} \approx \frac{1}{\sum_{k=1}^{\eta} m_{i_k} \sum_{k=1}^{\eta} m_{j_k}}$$
$$\cdot \sum_{k_1=1}^{\eta} \sum_{k_2=1}^{\eta} m_{i_{k_1}} m_{j_{k_2}} \int_{v_{i_{k_1}}} \int_{v_{j_{k_2}}} \overline{\overline{G}}_A(r, r') \hat{\ell}_i \cdot \hat{\ell}_j dr' dr, \quad (21)$$

where L is a dense matrix of size $qn \times qn$. One immediately notices that the system setup cost associated with computing the integrals of higher-order basis functions as in (21) is actually the same as those involving piecewise-constant basis functions. Furthermore, the accelerated integration techniques introduced in [2] for piecewise-constant basis functions can still be applied to the higher-order basis functions introduced in this paper. More importantly, due to the fact that $q \ll \eta$, R and L matrices produced by the use of the specialized basis functions are much smaller in comparison to the use of piecewise-constant basis functions, which generate, instead, matrices of size $\eta n \times \eta n$.

IV. RESULTS

This section utilizes our specialized high-order basis functions to efficiently extract the impedances of various complex IC structures. The basis functions are implemented in an EM solver where a pre-corrected FFT (pFFT) scheme [3] is introduced for the accelerated matrix-vector products involving dyadic Green's function kernels so that substrate effects can be accounted for. The specialized basis functions' efficiency is validated by comparing their performance to that of piecewise-constant basis functions.

A. Stacked Inductors

A set of specialized basis functions is first pre-computed in the frequency range of $[0.01MHz \dots 10GHz]$ for trial copper wires with rectangular cross-sections that are $5\mu m$ thick and $10\mu m$ wide. Subsequently, impedance analysis utilizing the specialized basis functions is performed on four structures as shown in Fig 2.a,b,c,d, where each structure is embedded in a silicon oxide dielectric ($\varepsilon_r = 3.9$) above a silicon substrate ($\varepsilon_r = 3.9$, $\rho = 1\Omega \cdot cm$).
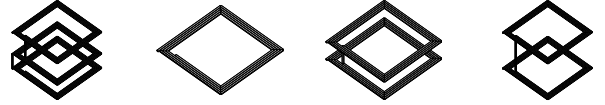

Fig. 2. a. A three-layer M3-M2-M1 inductor. b. A one layer M3 inductor. c. A two-layer M3-M2 inductor. d. A two-layer M3-M1 inductor.

For the three-layer M3-M2-M1 inductor in Fig. 2.a, the vertical heights of its three spirals are $16\mu m$, $26\mu m$ and $36\mu m$, respectively, above the silicon substrate. The single-layer M3 inductor in Fig. 2.b is composed from the topmost layer of the inductor in Fig. 2.a. The M3-M2 inductor of Fig. 2.c is composed from the top and middle layers of the three-layer inductor. The M3-M1 inductor of Fig. 2.d is composed from the top and bottom layers of the same three-layer inductor. In turn, each inductor spiral is composed of a 4-turned copper wire that is $5\mu m$ thick and $10\mu m$ wide with a lateral dimension of $0.25mm^2$ and a separation distance of $2\mu m$ between metal windings.

Fig. 3 shows the error generated from the utilization of the high-order basis functions in comparison to the solution obtained from a fine piecewise-constant discretization scheme. For a maximum absolute error of only 0.25%, 8 specialized basis functions per conductor segment are needed in contrast to the requisite 48 piecewise-constant basis functions per segment to obtain the same amount of accuracy.
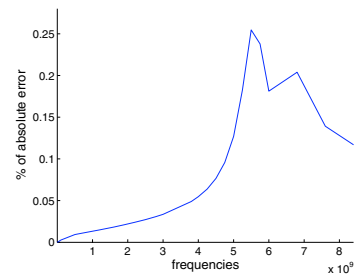

Fig. 3. Error analysis for the usage of specialized high-order basis functions. Analysis is performed on the single-layer inductor example.

The factor of 6× reduction in the number of basis functions translates to a significant 36× reduction in the computational cost of near-distance interactions when solving the system in a pre-corrected FFT (pFFT) scheme. This fact is confirmed by the FLOP (floating point operation) count decomposition in Table. I for each major stage of the pFFT scheme as it is applied to our single-layer inductor example.

Note that even though the cost of assembling projection (P) and interpolation (I) matrices is only reduced by a factor of 8.6 for the use of higher-order basis functions, there exists a dramatic 36.28× reduction in the cost of pre-correction, an observation that matches our theory that by reducing the

	piecewise-constant	Higher-order	reduction factor
# filaments	720	120	6
P and I matrices	1.9e5	2.3e4	8.3
D matrix	1.1e9	6.8e8	1.6
Pre-correction matrix	1.27e10	3.5e8	36.3
Iterative solve	1.18e8	9.4e6	12.6

TABLE I

FLOP COUNT FOR THE ASSEMBLY OF EACH pFFT STAGE FOR FILAMENT POTENTIAL CALCULATIONS OF THE SINGLE-LAYER INDUCTOR AT FREQUENCY=1GHz.

Fig. 5. Structural view of an array of 8 conductors with (a). trapezoidal cross-sections and (b). rectangular cross-sections.

overall number of basis functions by a factor of N, one is able to reduce the cost of resolving nearby interactions, which cannot take advantage of the acceleration offered by pFFT, by a factor of N^2 as manifested at the pre-correction stage. Furthermore, the cost of iterative solve is reduced by a factor of 12, which is approximately O(Nlog$N$).

Additionally, Fig. 4 shows the quality factor analysis of the four inductor structures in this section.
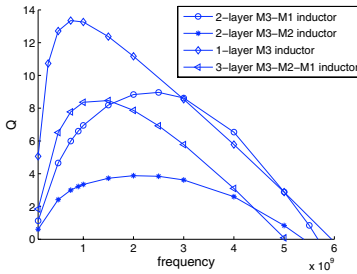

Fig. 4. Quality factor analysis for the four inductors.

Their overall simulated behavior confirms the research conducted by [15] which theorizes that a stacked spiral inductor's self-resonance frequency (f_{SR}) can be drastically modified by the vertical placement of its spiral layers, and in some cases, by as much as 100%. Typically, a stacked structure exhibits a single $f_{SR} = \frac{1}{2\pi\sqrt{L_{eq}C_{eq}}}$, where L_{eq} and C_{eq} are the equivalent inductance and capacitance of the structure, respectively. Generally speaking, the inter-layer capacitance between the spirals has a much greater impact on f_{SR} than the layer-to-substrate capacitance. Hence increasing the stack separation distance diminishes the inter-layer capacitance while maintains a relatively constant inductance because the lateral dimensions of a stacked inductor are nearly two orders of magnitude greater than its vertical dimension. Results in Fig. 4 confirm that this is indeed the case for our inductor examples. One observes that f_{SR} of the M3-M1 inductor is 25% greater than that of the M3-M2 inductor. Even more dramatic is the fact that f_{SR} of the M3-M1 inductor is 100% greater than that of the M3-M2-M1 inductor.

B. Conductor Array with Trapezoidal Cross-sections

A second set of specialized basis functions is pre-computed in the frequency range of [1$MHz\ldots40GHz$] for trial copper wires with trapezoidal cross-sections that are 1.2μm thick, 1μm wide on the top base and 0.6μm wide on the bottom base. Subsequently, impedance analysis is performed on an 8-conductor bus example with each conductor 300μm in length and separated 2μm from the neighboring wires. Fig. 5.a offers a zoomed view of such configuration. The entire structure is embedded in a dielectric ($\varepsilon_r = 3.9$) and situated 16μm above a conductive substrate ($\rho = 0.1\Omega \cdot cm$, $\varepsilon_r = 11.7$).

Due to the combined effects of irregular cross-sectional shape and skin and proximity phenomenon, each conductor's trapezoidal cross-section must be discretized finely if piecewise-constant basis functions were used. This concept is illustrated by the fine cross-sectional mesh shown in Fig. 5.a. To be specific, 104 piecewise-constant filaments per conductor are required for this particular example. In contrast, only 8 specialized higher-order basis functions are needed to capture the same conductor cross-sectional current distribution for a maximum error of only 0.0072% as shown in Fig. 6.
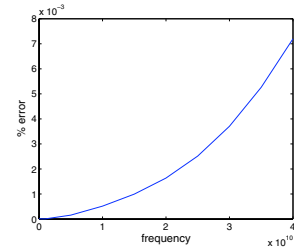

Fig. 6. Error analysis for the usage of higher-order basis functions.

This is a factor of $13\times$ reduction in the number of basis functions, which translates to a reduction of $169\times$ in the computational cost of near-distanced interactions when solving the system in a pre-corrected PFFT scheme. FLOP count analysis in Table II confirms such claim. For the use of higher-order basis functions, the cost of constructing P and I matrices are reduced by a factor of 17, the cost of D matrix construction is comparable to that of piecewise-constant basis functions, but the cost of pre-correction is reduced by a factor of 170 and the cost of solving the system using an iterative method is reduced by a factor of 108.

	piecewise-constant	Higher-order	reduction factor
# filaments	832	64	13
P and I matrices	2.3e5	1.3e4	17.7
D matrix	2.8e9	1.6e9	1.8
Pre-correction matrix	1.7e10	1.0e8	170
Iterative solve	1.3e8	1.2e6	108.3

TABLE II

FLOP COUNT FOR THE ASSEMBLY OF EACH pFFT STAGE FOR FILAMENT POTENTIAL CALCULATIONS OF THE CONDUCTOR ARRAY EXAMPLE AT FREQUENCY=1GHz.

To further demonstrate the versatility of our solver, we can compare the impedances extracted for the trapezoidal example to those extracted for the case where the conductors have rectangular cross-sections (1.2μm thick and 0.8μm wide). Such configuration is shown in Fig. 5.b. The simulation setup is such that resistance and inductance are extracted under the condition where the two center conductors are shorted at one end, while capacitance extractions are performed under an open-circuit condition. The resulting resistance, inductance,

and capacitance comparisons are shown in Fig. 7.a, b, and c, respectively.
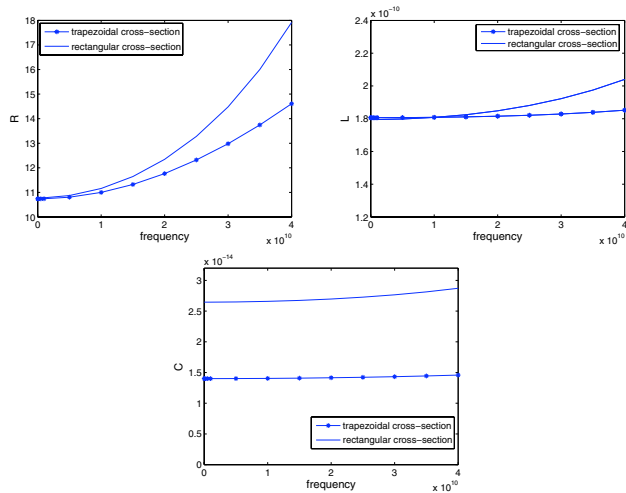

Fig. 7. Comparisons of (a) resistance, (b) inductance and (c) capacitance between the 8-conductor array with trapezoidal cross-sections and the array structure with rectangular cross-sections.

V. CONCLUSION

In this paper we have described a procedure for the numerical construction of shape-unique basis functions that are capable of parameterizing the frequency-dependent nature of a conductor's cross-sectional current variation, hence capturing electromagnetic phenomenon such as skin and proximity effects with fewer degrees of freedom in comparison to the commonly-used piecewise-constant basis functions. The frequency-independent nature of the basis functions implies that they only need to be pre-computed once for each unique cross-section shape and are valid over a pre-specified range of frequencies. In addition, these basis functions have proven to be robust and computationally efficient. Examples have conclusively demonstrated that the use of these basis functions achieves a 36 to 170 factor of reduction in the cost of solving large and intricate interconnect systems when compared to the use of piecewise-constant basis functions.

ACHNOWLEDGEMENT

REFERENCES

[1] M. Kamon, M.J.Tsuk and J.K. White. "FASTHENRY: a multipole-Accelerated 3-d inductance extraction program." *IEEE trans. microwave theor. tech.,* vol. 42, no.9, Sept. 1994.
[2] X. Hu, J. Lee, J. White, and L. Daniel. "Analysis of full-wave conductor impedance over substrate using novel integration techniques." *DAC,* California, June 2005.
[3] J.R. Phillips and J.K. White. "A precorrected-fft method for electrostatic analysis of complicated 3-d structures." *IEEE Trans. IEEE trans. comput.-aided des. integr. circuits syst.,* Vol 16, no. 10, Oct. 1997.
[4] S. Kapur and D. Long. "Large scale capacitance calculations." *DAC,* California, June 2000.
[5] Z. Zhu, B. Song and J.K. White "Algorithms in FastImp:a fast and wideband impedance extraction program for complicated 3-D geometries." *IEEE Transaction on Computer-Aided Design of Integrated Circuits and Systems* Vol.24, No.7, July.2005
[6] N. Marques, M. Kamon, L.M. Silverira and J.K. White. "Generating compact, guaranteed passive reduced-order models of 3-D RLC interconnects." *IEEE Transaction on Advanced Packaging*, Vol. 27, No.4, Nov 2004.
[7] A.E. Ruehli. "Equivalent Circuit Models for Three Dimensional Multiconductor Systems." *IEEE trans. microwave theor. tech.,* Vol. 22, March 1994.
[8] P. Silvester. "Modal network theory of skin effect in flat conductors." *Proc. of IEEE,* Vol 54, No. 9, Sept. 1966.
[9] M.J. Tsuk and J.A. Kong. "A hybrid method for the calculation of the resistance and inductance of transmission lines with arbitrary cross section." *IEEE trans. microwave theor. tech.,* Vol 39, No. 8, Aug. 1991.
[10] K.M. Coperich, A.E. Ruehli, and A. Cangellaris. "Enhanced skin effect for partial-element equivalent-circuit (PEEC) models." *IEEE trans. microwave theor. tech.,* Vol. 48, No. 9, Sept. 2000.
[11] J.Wang, J. Tausch and J.K. White "A wide frequency range surface integral formulation for 3-D RLC extraction." *ICCAD*, pp.453-457, San Jose, CA, 1999.
[12] L. Daniel, A. Sangiovanni-Vincentelli, and J. White. "Using conduction modes as global basis functions for efficient electromagnetic analysis of on-chip and off-chip interconnect." *DAC*, California, June 2001.
[13] L. Daniel, A. Sangiovanni-Vincentelli, and J. White. "Proximity templates for modeling of skin and proximity effects on packages and high Frequency interconnect." *ICCAD*, California, 2002.
[14] R.F. Harrington. *Field Computation by Moment Methods.* MacMillan, 1968.
[15] A. Zolfaghari, A. Chan and B. Razavi. "Stacked inductors and transformers in CMOS technology." *IEEE J. Solid-state Circuits*, Vol.36, No.4, April 2001.